Soft Piezoresistive Sensors for Distributed Sensing

Amir Firouzeh, Antoine Foba Amon Junior, Jamie Paik

Reconfigurable Robotics Lab Ecole Polytechnique Federale de Lausanne EPFL-STI-IGM-RRL Station 17, Lausanne, Switzerland

Abstract

Recent robots target safety, reconfigurability and interactivity by addressing the "soft" aspect of the hardware either by endowing additional degrees-of-freedom or through inherent compliancy. These robots require distributed sensing with flexibility and softness that would not interfere with the robot's agility. There have been various sensing solutions using soft conductive materials including conductive silicone, liquid metal-filled micro channels, and conductive-ink based sensors. However, we still lack a comprehensive study on their potentials, drawbacks, and the different parameters that affect their response.

In this paper, we present our design, fabrication process and characterization results for conductive silicone polymer and carbon ink-based curvature sensors. These sensors are flexible, mechanically robust under large strains, scalable, and easy to fabricate in large numbers. The proposed model in this work is unique for its extensive characterization of these polymer-based sensors and for its systematic categorization to compare performance of conductive silicone and carbon ink-based sensors with different design parameters.

Keywords: Soft sensor, carbon polymer composite, sensor modeling, sensor characterization, Piezoresistivity, printable sensors, conductive silicone sensors.

1. Introduction

Applications that require interacting with humans and operating in unknown environments are motivating more compliant systems with many discrete or continuous degrees-of-freedom (DoF). New methods for soft and scalable actuation [1, 2, 3] and

sensing [2] have made this transformation from rigid body robots to soft and reconfigurable systems possible. But the capabilities and limitations of these emerging components have not been thoroughly studied. Figure 1 presents two examples of applications that benefit from an array of flexible low-profile sensors . These applications are based on Origami robot, Robogami, [4] which is a low profile robotic sheet that can reconfigure its form by folding actively (in the case of the crawler robot [2] figure 1(a)) or deform passively and provide feedback on the shape (the case of the facial rehabilitative device [5] figure 1(b)). In both of examples, accurate feedback on the joint angle is necessary. In this research, we elaborate on the performance analysis of soft and flexible curvature sensors that can be used in such applications. We report on the major characteristics of the two classes of sensors and suggest a model to explain their behavior. Using the result of the characterization tests, we compare the performance of these sensors.

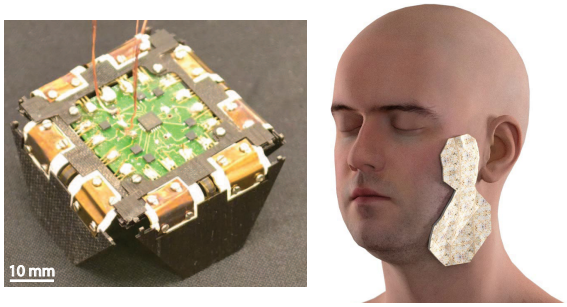

(a) (b)

Figure 1: Two examples of the applications of the flexible curvature sensor arrays: the Crawler robot [2] that uses a curvature sensor on each leg (a), and a Robogami conceptual design for an assistive device for assessing the paralysis level in the patients with facial palsy [5] (b).

Flexible strain sensors work on different principles including the change in the capacitance [6, 7, 8] or resistance [9] in a solid-state material or change in the resistance caused by the shape change in liquid metal-filled micro-channels [10]. Between these, the piezoresistive based sensors have a very simple fabrication process and need

a rather primitive auxiliary circuit. This makes them highly scalable [11] and more appropriate for arrays of sensors consisting of many sensing elements. When piezoresistive sensors undergo strain, the conductive paths made by the conductive particles break down and their electrical resistance increase. In general, the sensing material is made from conductive particles in a non-conductive soft polymer matrix. One family of these sensors are made by impregnating different rubbers with carbon particles [12, 13]. This conductive paste can later be molded into a desired shape as suggested in [2]. The ease of fabrication in large arrays is one the main advantages of this type of sensor. Another family of strain sensors are based on a carbon layer deposited on polymer sheets [14]. The carbon layer usually contains a hard polymer as the matrix. In this research the performance of these two families of sensors will be studied in detail.

The behavior of the carbon particle-based sensors can be studied on micro-scale [15, 16, 17, 18] or on macro-scale [19, 20, 21]. The study of the interaction of carbon particles and the polymer matrix on the micro scale is interesting for understanding the nature of different phenomena and optimizing the component choices. In the second approach, a gray box model is used to explain the relation between the resistance and strain. This type of modeling is more attractive for those who are concerned with the bulk response of the sensors. Such a model is still useful in optimizing the design parameters [21] of the sensor since the elements that make up the model are representative of the characteristics of different components that make up the sensor [19]. To characterize the sensors, researches in both groups mostly studied cyclic loading with fixed loading rate [22, 23]. Some researchers also studied the dynamic response of these sensors [19, 15]. Still some effects such as drift or creep [17] were not studied thoroughly. A model in macro scale [19] that explains all these effects would provides us with a set of figures of merit for comparing the performance of different sensors [24, 25]. Although the main focus of this work is on presenting a model in the macro scale, we try to attribute physical meaning to the parameters in the model. Among the theories suggested for the resistance change of piezzoresistive materials the theory based on the destruction of conductive pathes [26, 27] is the one that can explain the increase in the resistance of the material under compression. This theory explains the overall behavior of the sensors (increasing the resistance regardless of the direction

of bending) and also through this theory the transient response of the sensor and the suggested equivalent mechanical model is explained.

The major contributions of this research are:

- Presenting customizable piezoresistive sensor designs and fabrication methods suitable for distributed sensing applications.
- Characterizing and modeling these sensors which are necessary for preparing a guideline to choose the sensor most fit for different robotic applications.
- Exploring the less studied aspects of the behavior of the piezoresistive based sensors. The three aspects of the sensor response studied here are: the dynamic response, the drift in the sensor reading, and the accuracy and precision of the response in cyclic loading.
- Presenting a mechanical equivalent model to explain sensor behavior.
- Introducing a set of figures of merit based on the model and the test results for sensors with different designs and components.

Section 2 of this manuscript presents the fabrication process of the sensors. In Section 3, the setup for characterization tests is introduced and in Section 4, a model that can explain the behavior of the sensors is presented and a set of tests for evaluating important parameters in the model are presented. In Section 5, the results of the characterization tests are presented and the effect of material choice and fabrication process are discussed. Finally, the conclusion of this work and the future steps are presented.

2. Fabrication process

In this paper, we study two families of piezoresistive sensors: *Carbon silicone composite* (CSC) and *carbon ink* (CI) sensors. Under strain, due to relative motion of the conductive particles, that make the conductive paths, the overall electrical resistance of the sensing material changes. Although the working principle is quite similar, the appearance, mechanical properties, and fabrication process of these sensors are very different. The main advantages of the CSC sensors are their ease of fabrication and

robustness in extreme loading conditions (upto 100% strain). The main advantage of the ink-based sensors is their better transient response, lower drift, and better accuracy as will be discussed in section 5. In what follows, we describe the fabrication processes of these sensors in detail.

2.1. Conductive Silicone Composite (CSC) Sensors

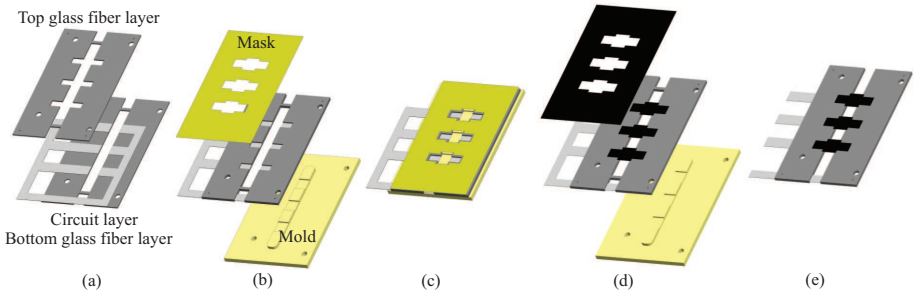

Figure 2: Fabrication process of the conductive silicone sensors. (a) In the first step, the patterned pre-impregnated glass fibre and conductive fabric (which makes the circuit and the sensors electrodes) are stacked and cured in a heat press at 135°C for 30 minutes. (b,c) In the second step, the sensor base is fixed on a 3D printed mold and is covered with a mask layer. The mold makes the shape of the sensors more uniform and the mask makes cleaning and isolating the sensors easier in the subsequent step. (d) Next, the conductive polymer layer is cast and placed in the oven for curing. Finally, the module is released from the mold and the mask is lifted off. (e) Finally, the connections to the four leads of the electrodes are cut. As illustrated in the figure, in this module, we have three sensors in parallel.

The fabrication process of the CSC sensors starts with laser micro-machining (the process introduced in [2]) of the components needed for the base (pre-impregnated glass fiber layers and conductive layer). Then, these components are stacked and cured in a heat-press to form the base for the sensors. In the current design, we make three sensors on each module to study the repeatability of the fabrication process. We use a 3D printed mold and a mask as presented in figure 2 to better control the thickness and the shape of the sensors during the casting of the sensing material. The size of the

carbon particles used in the CSC are 42 *nm* (39724 from Alfa Aesar). Under strain, the conductive links in the CSC made by these particles break, causing an increase in the electrical resistance of the sensor. It is expected that the polymer properties and the mass ratio of the carbon particles in the mixture would affect the response of the sensors. To study the effect of the polymer properties, we test two silicone rubbers with different mechanical properties: Ecoflex 0030 and Dragon Skin 30 (from Smooth-on). The latter is around 10 times stiffer (600 *kPa*) than the former (69 *kPa*) [28]. As for the mass ratio, as suggested in [19], there is compromise between sensitivity and conductivity. For the Ecoflex sensors and the Dragon skin sensors 5.5% and 7.5% carbon to silicone mass ratio, respectively, give acceptable results which will be presented here. To achieve a more uniform mixture, we also added 15% mass ratio of n-Hexane solvent to reduce the viscosity of the mixture. After casting the silicone, the module is placed in a vacuum chamber to degas the polymer. Then it is placed in an oven at 70°C to cure the polymer. These steps are illustrated in figure 2.

2.2. Carbon Ink (CI) Sensors

The change in the conductive paths under strain is the working principle for both the CI sensors and the CSC sensors. In a sense, the CI sensors can be regarded similar to the CSC sensors but with much stiffer matrix material. The choice of the matrix and the substrate material influences the performance of the sensors. polyimide film was picked as the substrate material based on its desirable chemical, thermal and electrical characteristics. The thickness of the polyimide substrate determines the strain in the ink layer. Based on the compromise between the sensitivity and the accessible range of deformation (the ink layer can sustains unrecoverable damage in small radii of curvature as the polyimide layer becomes thicker and the strain in the ink increases). Given our goal for reaching 1.3 mm radius of curvature, we chose 50 μm thick polyimide sheet as the substrate which gave good results in the experiments. As for the ink, different compositions were studied and based on their performance, a water based ink with micron size particles (PELCO conductive ink No. 16051 [29]) was chosen.

The piezoresistive materials in general are highly sensitive to ambient conditions, like humidity and temperature and it is necessary to encapsulate the ink layer with

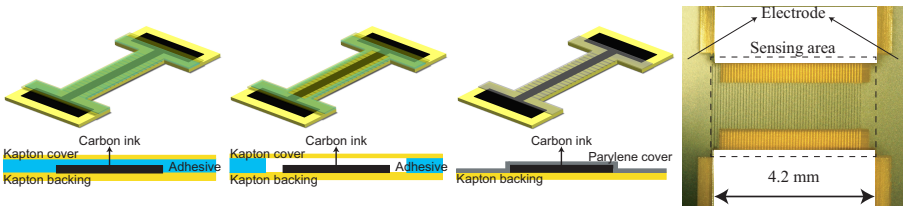

Figure 3: Three different types of CI sensors: Sensor with polyurethane and polyimide layer, CI1 (a). Sensor with polyurethane and polyimide layer, CI2 (b). The ink and the polyurethane are not in contact in CI2. Sensor with parylene coating, CI3 (c). A microscopic image showing the score marks on the substrate (d).

a barrier to minimize the error caused by change in the surrounding condition. The cover material changes the behavior of the sensor and here to find the cover that gives the best results, we have considered three options. The first cover layer studied was a polyimide thin layer (13 μm) bonded on to the substrate and the ink layer using polyurethane hot-melt (figure 3(a)). In another version, the same combination was used but the polyurethane layer was cut with a pattern to prevent contact between the polyurethane layer and the ink layer in the sensing area (figure 3(b)). The last type is fabricated by covering the sensor with a thin (2 μm) parylene layer (figure 3(c)).

The fabrication process for the CIs starts with scoring the surface of the polyimide sheet with the laser up to half its thickness along the area which will make the sensitive part of the sensor. The width of the score marks is same as the beam size of the laser which is 30 μm. These notches on the polymer layer will provide points of stress concentration and hence increases the sensitivity of the sensor (the first step in figure 4). Next, a uniform layer of carbon ink is deposited on the polyimide sheet using a brush made of fine glass fibre fabric. After the ink gets cured, we burn the ink on the side of the sensitive part in order to make anchoring areas for the cover layer as presented in the second step in figure 4 . Up to this point, the fabrication process of all three sensors are the same. In the third step, two of the sensors (CI1 and CI2) are covered with polyurethane (100 μm thick before pressing) and polyimide (13 μm thick) layers

and get laminated in a heat press at 160°C. The difference between CI1 and CI2 is in the shape of the polyurethane layer. In CI1 the polyurethane layer covers the whole sensor surface, in CI2 however, this layer is cut to prevent contact with the ink layer. The characterization test result confirmed that CI2 has the best performance among the tested sensors. Next, the outline of the sensors are cut with the laser and the wires are attached to the electrodes. We also experimented with parylene coating instead of polyurethane and Kapton (CI3) since we expected that the reduced thickness of the coating would improve the result. Eventually, the sensors are embedded in patterned glass fiber layers (as presented in figure 2(a)).

3. Experimental setup

To characterize the sensor response, we fabricated a motorized test stage (see figure 5(a)). A stepper motor with a step size of 1.8° regulates the bending in the sensors. The resistance change in the sensor is transformed to a voltage change using the circuit presented in figure 5(b). For the CSC sensors, the electrical resistance change is high enough and only an OpAmp with a simple voltage follower circuit will be used between

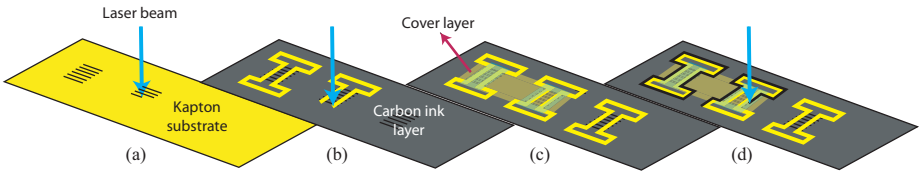

Figure 4: Fabrication process of the CI sensors. In the first step, the surface of the polyimide sheet is scored by the UV laser (a). Next, a layer of carbon ink is deposited on the polyimide and after curing, in the second step, the anchoring points around the sensing area are cleaned by burning the carbon layer with laser (b). In the third step, the polyurethane cover layer is added (for the two sensors on the left: one with polyurethane covering the whole surface including the entire surface of the ink layer and another with polyurethane just covering the extremities) (c). Finally, the outline of the sensor is cut out and the wires are attached to the electrodes (d). For the parylene coated sensors, the final product is covered with a thin parylene layer.

the sensor output and the Data Acquisition card (DAQ). But for the CI sensors, we need to amplify the voltage 100 times to make the signal noise ratio (SNR) sufficiently large (SNR of more than 50 was considered acceptable). The data acquisition card (NI USB-6009) collects the data at the rate of 100 Hz. Having a rather fixed condition throughout the experiments, we used a simple resistor for dividing the voltage. In different applications, one can replace the voltage divider resistor with a control sensor (with the same properties and in the same condition as the test sensor but not under strain) to minimize the effect of the environmental conditions.

4. Modeling and characterization

The models presented for polymer based piezoresistive sensors mostly focus on the steady-state response but neglect some aspects of the sensor response such as drift in a large number of cycles. In this section, we present a model that can explain the main aspects of the sensor response. By determining the important parameters in this model, we will have a basis to compare the performance of different sensors. More over, by interpreting the physical meaning of the elements in the model, we will acquire a guideline for improving the design of the sensors. Figure 6 presents the sensor model.

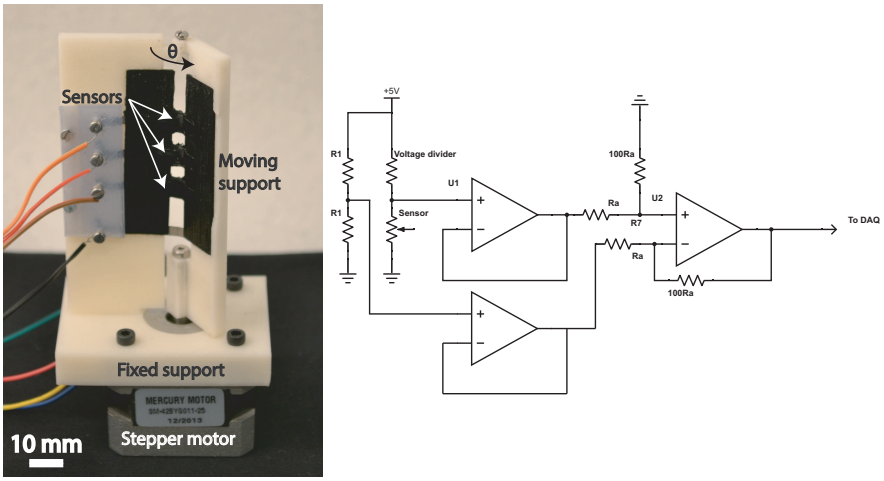

Figure 5: Sensor test set-up: the motorized stage used for bending the sensors (a), the voltage divider and the amplification circuit with the amplification ratio of 100 (b).

In this model, the carbon particles are presented in black and the polymer matrix is presented by blue carts that are connected with a combination of dampers and springs. The elements of the model are chosen so it would represent the two main characteristics of the sensor response: the transient response and the amplitude dependent drift in the sensor reading. This drift is referred to as recoverable drift through out the text. In a perfect sensor, these two effects should be negligible. But due to the inherent material characteristics, all polymer based sensors display these effects to different extent.

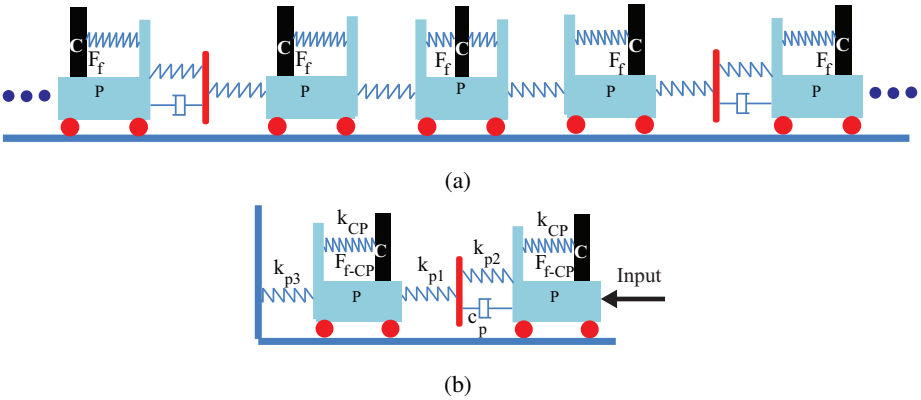

Figure 6: The equivalent mechanical model for sensors (a). The simplified model where all the elements with same effect are lumped into one equivalent element (b). In this model, black blocks represent the carbon particles (labeled **C**) and the distance between them is translated to the resistance change of the sensor. The carts and the connecting spring and dampers represent the polymer matrix (labelled **P**). The friction force between the carbon particle and the polymer matrix and the force in the spring that is labeled **CP** are the forces between the carbon particles and the polymer matrix.

Here, we examine three different aspects of the sensor response. First, we study the transient response of the sensors which is governed by the dynamics of the polymer matrix (presented by components with **P** label in figure 6). Next, the recoverable drift in the sensor reading is studied which is governed by the interaction between the polymer matrix and the carbon particles (modeled by the components with **CP** label in figure 6). Finally, the quasi-static response of the sensor will be investigated. The result of this

will enable us to translate the movement of the particles (strain) in the equivalent model to the resistance change in the sensor. As previously suggested in [19], the transient response of the sensors can be attributed to the polymer's visco-elasticity. The friction force introduced between the carbon particles and the polymer matrix causes the drift in the position of the carbon particles in repeated cycles. This drift in particle position reflects the drift observed in the resistance of the sensors in repeated cycles. The study of the model suggests that the drift part of the response is only dependant on the fast movements in the matrix and not on the slow relaxation and moreover the transient response of the sensors is not dependant on the recoverable drift. Based on this, these two parts of the model can be studied separately. In what follows, we present the test procedure for characterizing different behaviors of the sensors. In CSC, the transient response can affect the recoverable drift to some extent, but the test is designed so that the two effects can be studied separately.

4.1. Transient response

The transient response of the sensors is caused by the visco-elastic behavior of the polymer. This behavior is modeled using a combination of springs and dampers. In the proposed model, we have added more elements compared to other models, such as [19], so it would represent the behavior of the sensor more closely. The transient response of the sensor is caused by a combination of normal and lateral strain in the material. Considering the normal strain as the input, the change in the lateral deformation caused by overall volume change is what causes the transient response in the sensors.

The characterization test for this part of the model is composed of two tests: first, loading the sensor from relaxed (0°) to a half closed position (90°) with a step input (approximated by a ramp loading with 0.5 s rise time): second, unloading the sensor from completely closed state (162° for CIs and 144° for CSCs) to (90°). For the CSCs bending over 144° would cause the two sides of the sensor to come in contact. Figure 7 presents the response of the CI2 sensor in these two tests.

One of the interesting features in the response of the sensor is that both in loading and unloading, the sensor reading decreases over time after the deformation. In this section we model this effect by an equivalent mechanical system of figure 8. where

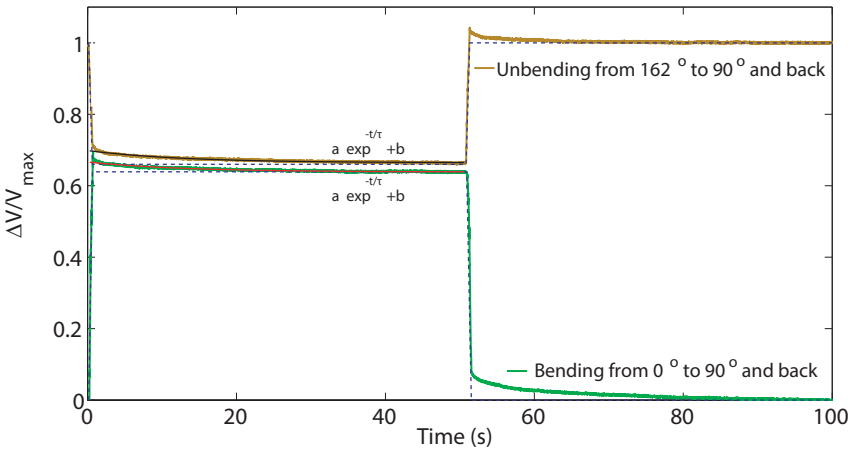

Figure 7: The transient response of the CI2 in moving from 0° to 90° (green line) and from 162° to 90° (brown line). Both on the rising and the falling edges the resistance decreases over time. This can be attributed to different effects such as the lateral deformation in the sensor. As shown, we model this response using the first order dynamics.

the input deformation, causes two displacements of interest which can be attributed to the volume change in the material x (an indication of the particle distance in the direction of the main deformation) and the lateral displacement u. As mentioned in the introduction, the lateral deformation causes increase in the resistance which can be explained by the theories based on the destruction of conductive network[26, 27]. So in the proposed model, the lateral deformation regardless of the direction of the input deformation would cause an initial resistance increase which over time vanishes as the lateral deformation decreases. We should point out that the same model can also explain the resistance increase of the piezoresistive materials under the pressure. Based on this model, we present the resistance of the sensor as:

$$R = R_1(x) + R_2(|u|) = r_1 x + r_2|u| \tag{1}$$

Here we have assumed that the resistance is a linear function of the displacement. As will be seen in the quasi-static characterization of the sensor, this assumption is not true for the whole range of motion but it can be used in finding a measure of performance for the sensor around a specific point.

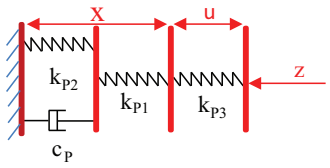

Figure 8: The transient response components of the sensor model. The portion with the displacement x is the standard model that is used for modeling creep and viscoelastisity in the polymers. The displacement in the third spring denotes the lateral strain in the material which causes the effective conductive paths to break. The input to the model is the displacement z and the outputs are x and u.

Based on this model, we have the following expressions for the displacements of interest:

$$\begin{aligned} X(s) &= (\frac{1}{A} + \frac{1}{B+DS})Z(s) & x(t) &= ae^{-t/\tau} + b \\ & \rightarrow & & \\ U(s) &= (\frac{A-1}{A} - \frac{1}{B+DS})Z(s) & u(t) &= -ae^{-t/\tau} + (1-b) \end{aligned} \tag{2}$$

Using the test results presented in figure 7, we can evaluate the parameters in (2) but at the moment we are more interested in finding a tangible measure of performance for the sensors. So the parameters we report for each sensor are the time constant of the first order dynamic model (τ) and the normalized amplitude of the transient response in rising and falling edges (a_{r_n} and a_{f_n} respectively) which are defined as:

$$a_{r_n}(\%) = \frac{a_r}{a_s} \; and \; a_{f_n}(\%) = \frac{a_f}{a_s} \tag{3}$$

According to (3), the normalization should be carried out using the steady state amplitude of the resistance change but because of the non-linearities in the behavior of the sensor, the amplitude of the transient response is not necessarily dependent on the step size. So to have comparable values, for both the rising and faling edges we used the resistance change of the sensor as it bends from 0° to 90° for normalizing the readings.

Among the sensors tested here, only CSC1, which is composed of a very soft poly-

mer, exhibit a behavior different from what is presented in figure 7. For this sensor, we observe an initial increase in the sensor reading when it is moved back to the relaxed state as shown in figure 9. In this sensor, the damping effects are highly dominant which corresponds to a large value of the damping coefficient and comparably soft spring coefficient (this is linked to the softness of the polymer as expected). This causes large initial deformation in k_2 (which can be attributed to large lateral motion) and hence and initial increase in the resistance.

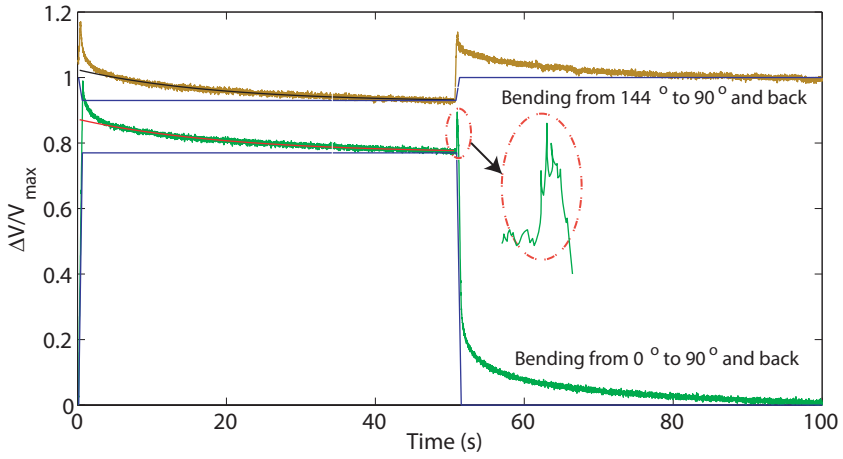

Figure 9: The transient response of CSC1 in moving from 0° to 90° and from 144° to 90°. The different aspect in the dynamic response of this sensor compared with the CI sensors (figure 7) is the initial increase in the resistance regardless of the direction of deformation. This point is emphasized in the plot by zooming in on the initial pick on the falling edge.

Figure 7 confirms that the first order dynamics accurately models the response of the CI2. This is not the case for CSC1 though (see Figure 9). The dynamic response for CSC1 can be better modeled by adding another stage composed of a damper and a spring but here we are more interested in slow portion of the transient response of the sensors (as they can cause bias in the readings during fast loading). Therefore, we represent the transient response with a first order dynamic model that captures only the slower portion of the dynamic response and compare the parameters of this model for

different sensors.

4.2. *Recoverable drift*

For most polymer sensors, due to the inherent soft material characteristics, drift in the sensor reading over time is inevitable. Though being neglected in many researches, this effect is one of the biggest drawbacks of the polymer based sensors. One part of this drift is irreversible and caused by the degradation of the sensor which according to the quasi-static tests, is not detrimental to the sensor performance. On the other hand, there is a reversible and significant drift in the sensor reading dependent on the *loading history*. The frictional force between the carbon particles and the polymer matrix is added to the model to capture this behaviour. Figure 15 presents a part of the general model (figure 6) that explains the recoverable drift in the sensors. The mechanical equivalent system of figure 15 that shows a drift in its response which is dependent on the elongation amplitude represents the model suggested for the sensor. The parameters of this model are the mass of the carbon particles, the friction force, and the spring constant.

In cycles of large bending angles, the positive work done by the spring and the friction in the first half of the cycle (figure 15 (a) to 15 (b)) is greater than the positive work when the polymer matrix goes back to the relaxed initial state (figure 15 (b) to 15 (c)). This will cause an offset in the position of the carbon particles in the end of a high amplitude loading cycle (figure 15(c)). When the sensor is later loaded with smaller amplitudes (figure 15(d)), the residue of the spring force would cause smaller positive work when the polymer gets stretched compared to the positive work when it shrinks back to its initial state. This will cause the particles to spring back to their initial state in the matrix in the repeated cycles (figure 15(e)). While the drift appears after the first couple of cycles with large amplitudes (after the first two cycles, the sensor readings would be similar for the rest of the cycles with high amplitude), the relocation of the particles to their initial state is a very slow process and many cycles of loading at small amplitudes are necessary to relieve the residual strain in the sensor.

Finding all of the parameters in the model requires extensive testing including loading in different rates. Here, we only report the normalized recoverable drift in the

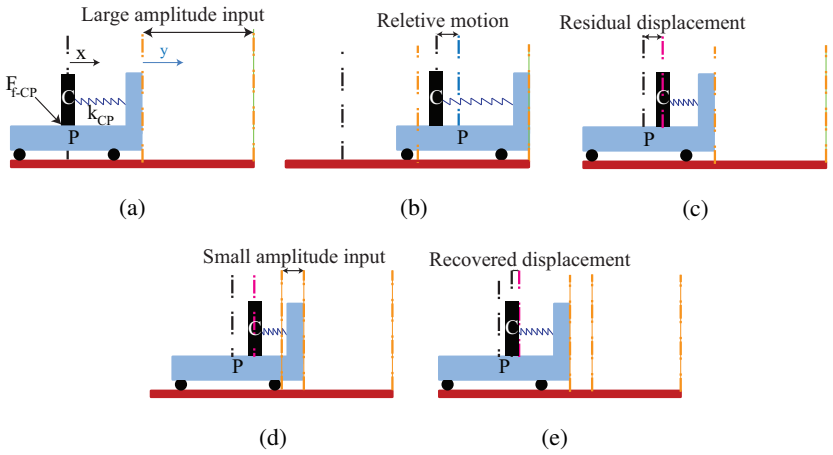

Figure 10: The portion of the model that represents the interaction between the carbon particles and the polymer matrix. The components in this part of the model were chosen to yield the same recoverable drift as is observed in the sensor reading. Initial state (a). Deforming the sensor with large amplitude (b). Polymer matrix returns to its initial state but carbon particles maintain some residual displacement (c). Deforming sensor with small amplitude. Because of the pre-strain in the spring, the carbon particle's displacement is small (d). Polymer matrix returns to its initial state after a small amplitude deformation and the carbon particles recover some part of the drift in their position (e).

sensor reading for one loading speed which provides us a measure of performance for comparing different sensors. The characterization test for this part begins with loading the sensor to the maximum for 20 cycles. Then the sensor is left at its relaxed state so that the transient response fades. Next, the sensor is loaded to 18° for 400 cycles. This angle is small enough so we can observe the drift recovery and large enough to exit the dead band of the sensor readings (it consists of 10 steps of 1.8°). In these repeated cycles the drift in the sensor reading is recovered little by little. In the final step of the test, the sensor is again left at rest to reach its steady state. Figure 11 presents the result of these tests for CI2. a_b in this figure presents the value we refer to as the recoverable drift in the sensor response.

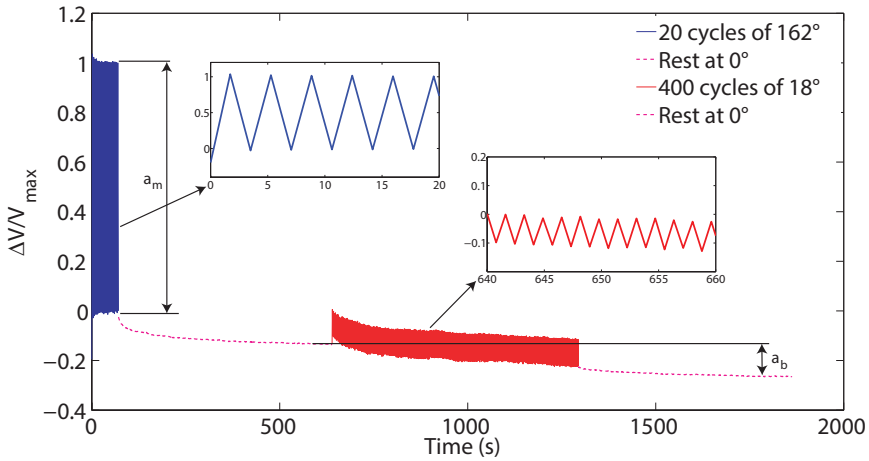

Figure 11: The drift in the sensor reading (CI2) caused by the loading amplitude. In this experiment, the sensor was loaded to the maximum bending (162°) angle for 20 cycles at first which causes the drift in the sensor. After that, the sensor was kept in the relaxed state so the transient response vanishes. Then in 400 cycles of 18°, the recoverable drift was relieved and the sensor is held steady again for the transient response to vanish. The voltage difference between the two steady state readings is a comparison measure we use for the recoverable drift in the readings.

To be able to compare the performance of different sensors we report the normalized bias amplitude for different sensors defined as:

$$ab_n(\%) = \frac{a_b}{a_m} \tag{4}$$

4.3. Quasi-static response

The quasi-static response of the sensor represents a measure of the repeatability of the readings and its accuracy. To study the repeatability of the readings, we bend the sensors in 18° increments between unfolded and folded states for 50 cycles and calculated the variance of the voltage reading in repeated cycles. We use the mean of the variance for all points to compare the quasi static performance of different sensors in repeated cycles ($\overline{\sigma_V}$). It should be pointed out that readings from the first cycle are different compared to all the following readings. This comes from the slow dynamics

of the sensor which causes the readings from the second cycle on to be slightly higher than that of the first cycle. Since in this section we only care about the repeatability of the sensor reading, we put aside this first cycle and calculate the variance based on the data from the remaining cycles. To give a comparable numbers for different sensors, we have normalized the error with the amplitude of the mean cycle of the readings. Figure 12 presents the result of this test for CI1.

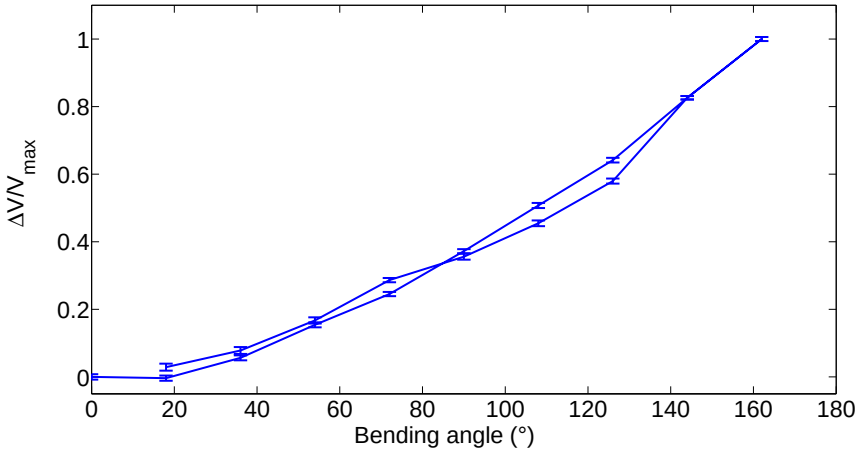

Figure 12: The quasi static response of the sensor (CI1) in 50 cycles with 18° step increments. The mean cycle and the variance are presented. The variance is a measure of the repeatability of the readings and the robustness of the sensors. For the ink based sensors with polyimide backing, the data is very coherent. The small hysteresis loop is another desirable aspect of these sensors response.

As mentioned above, other than dependency on the deformation, the drift in the CSC sensors also depends on the rate of deformation (at the current state we have not taken into account this dependency). The time intervals between steps in the quasi-static tests (0.5 s) is chosen so as that the drift caused by the loading rate would not be prominent but one should bear in mind that when used in applications with varying rate of loading, the results from the CSC sensors would be much less accurate [2]. The same effect for CI sensors is rather negligible.

The coherence of the data presents a measure of the repeatability of the tests and

the robustness of the sensors, but the accuracy of the sensor reading is also a function of the sensitivity of the sensor (the slope in figure 12). To study the accuracy of the sensors, a more detailed quasi-static test with increments of 1.8° was performed and a curve was fit to the data to give bending angle as a function of the voltage reading from the sensor.

The difference between the prediction of the fitted function and the actual bending angle provides us with a measure of the accuracy of the sensor around each bending angle. We use the mean of the standard deviations for all test point ($\overline{\sigma_\Theta}$) as the measure to compare accuracy of the sensors.

Another measure of the sensor performance is the width of its hysteresis loop. We present the maximum normalized *width* of the hysteresis loop which is the difference between the voltage on the rising edge and falling edge over the voltage amplitude of the whole cycle:

$$w_{Hys.n}(\theta) = \frac{|V_{rising}(\theta) - V_{fallin}(\theta)|_{max}}{V_{max} - V_{min}} \tag{5}$$

5. Results and discussion

In the previous sections, we introduced CSC and CI sensors. The working principle in these sensors is the piezoresitivity of carbon polymer composites material. We studied the response of these sensors and presented a model for explaining the behavior of these sensors. Also, a series of figures of merit were defined which are used in this section for comparing the performance of these sensors (presented in table 1).

In general, based on the model presented in sections 4.1 and 4.2, a polymer in which the elastic part of the response is more dominant compared to the viscous effects would give better transient response. Also, the use of a harder polymer as the matrix is expected to reduce the recoverable drift in the sensor since the conductive particles would follow the polymer matrix more closely. The comparison between the values in table 1 verifies these claims. Using harder polymers (EcoFlex in CSC1, Dragon Skin in CSC2 and carbon ink in CI2 and CI3 respectively) alleviates the drift and also improves the transient response. The latter is caused by the dominance of the elastic response compared to the viscous effects in the polymer.

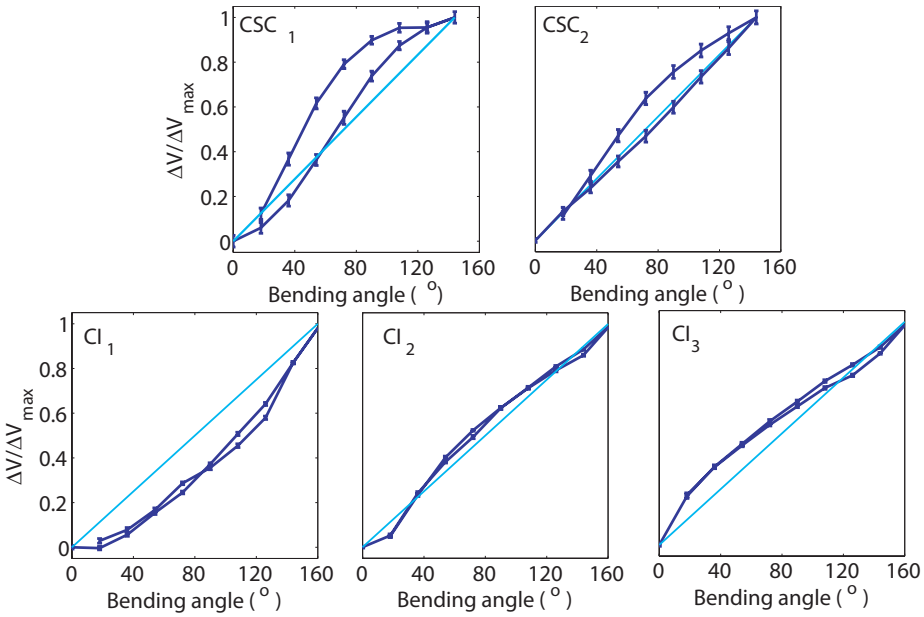

Figure 13: .

Among the ink based sensors, CI1 test results are exceptional and based on the numbers presented in table 1, CI1 has the worst transient response (based on the value of a_{f_n} and a_{r_n}). Also, its recoverable drift amplitude is quite substantial. In this sensor, the conductive ink is in direct contact with the polyurethane layer and it is partially transferred onto this layer while it is being laminated in the heat press during the fabrication. While the sensor is under strain the polyurethane layer moves with respect to the polyimide layer which breaks the conductive paths. The anchoring points added in the fabrication process, as presented in section 2.2, reduces this relative motion and significantly improves the result but it does not solve the problem entirely. The other two packaging techniques used (in CI2 and CI3) solved this problem and gave the best transient response and bias variation result among the tested sensors.

We should point out that table 1 is not showing the loading rate dependency of the bias in the CSC sensors which could be the most important drawback of these sensors. This, along with the uncertainty over the shape of the sensor (CSC sensors are too soft), are the main obstacles for successful application of conductive silicone curvature

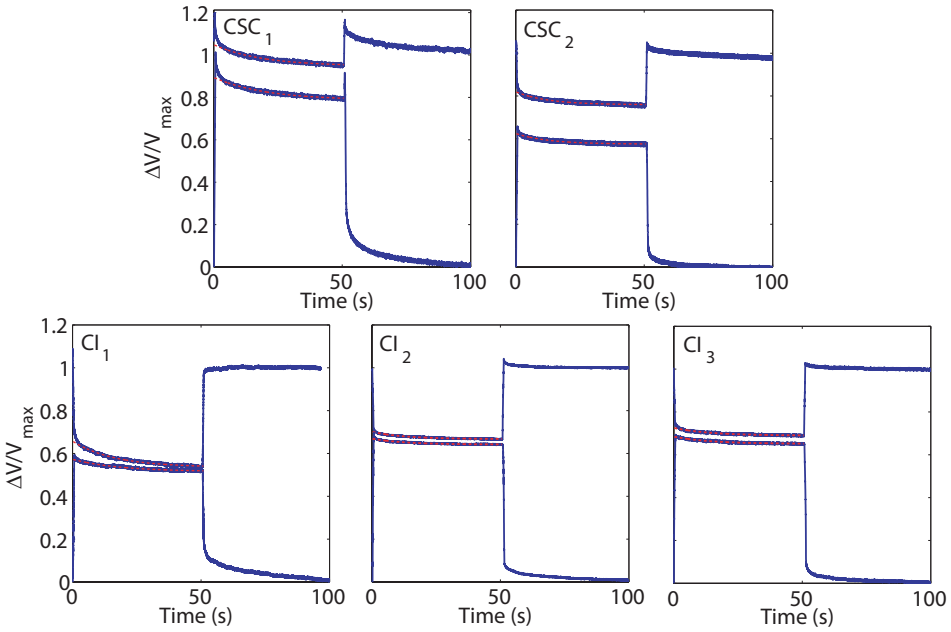

Figure 14: .

sensors [2].

In the quasi-static tests, the coherence of the measured data for the ink based sensors ($\overline{\sigma_V}$) is significantly better. This is mainly caused by the drift in the CSC sensors over time. Also, the shape of the CSC sensors are rather unconstrained compared to CI sensors that have a stiff polyimide backing. The accuracy of the sensor readings is not only a function of the coherence of the data but also the sensitivity in different regions. In general, CI sensors have more uniform sensitivity in their whole range of motion. This partly comes from their smaller hysteresis loop ($W_{Hys,n}$). Therefore CI sensors have smaller insensitive zones. Better sensitivity and coherence result in more accurate readings for CI compared to CSC sensors. CI1 has exceptionally poor performance among the ink based sensors which, as mentioned, is caused by the relative movement of the polyurethane cover layer. This causes both big hysteresis loop and an insensitive zone in small bending angles (a dead band) that results in a big variance.

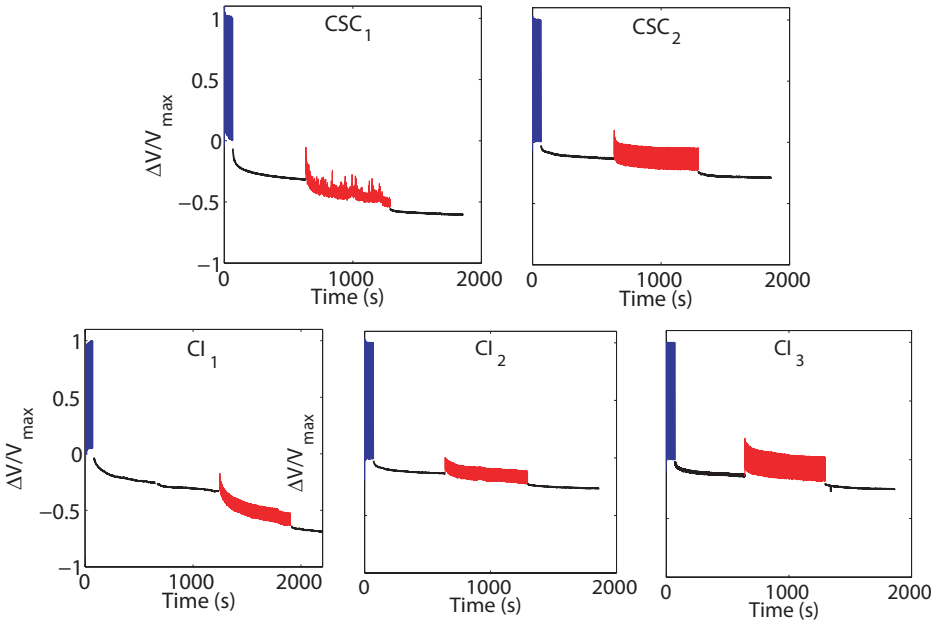

Figure 15: .

6. Conclusion and future work

In this research, we investigated the behavior of carbon particle-based curvature sensors, proposed a model to explain this behavior, and suggested a set of characterization tests to determine the important parameters in the model. Using the test results, a set of performance measures were calculated for each sensor and the proficiency of the sensors were compared based on these measures. To make comparison easier, we deigned three different tests each focusing on one aspect of the sensor behavior: the transient response, the recoverable drift, and the quasi static response. The main goal in the current study was to propose a systematic way of investigating the performance of different sensors. So we used the model for explaining the behavior of the sensors but instead of determining all the parameters in the model, we used a set of more tangible performance measures in each of the three categories of the characterization tests.

The sensors studied here can be divided into two families, the CSC and the CI sensors. The sensing principle in both groups is similar but in general ink based sensors have better performance in all three categories of characterization tests. From the com-

Table 1: Performance measure for different types of carbon particle based sensors.

	Transient response			Bias	Quasi-static response test		
Sensor type	τ(s)	$a_{r_n}(\%)$	$a_{f_n}(\%)$	$ab_n(\%)$	$\overline{\sigma_V}$ (%)	$\overline{\sigma_\Theta}$ (°)	$W_{Hys.n}(\%)$
CSC1	19.24	13.8	13	28.37	2.37	5.98	25.57
CSC2	12.5	9.0	10.9	15.76	2.48	2.65	17.33
CI1	17.1	10.7	23.5	39	0.75	2.67	8.2
CI2	12.78	4.4	5.3	12.95	0.55	1.05	2.9
CI3	14.22	5.2	5.6	11.42	0.67	0.89	4.2

parison between the results it can be inferred that the sensors that use harder polymers as matrix give better results in general.

We believe there is still room for improvement using inks with harder polymer as matrix. Also optimizing the score marks pattern on the polyimide base can result in better sensing behavior. Once the design of the sensor is optimized, a more detailed characterization can be performed to achieve an accurate model for the sensor. As an example, non-linearities in the sensor response that were neglected in this paper can be studied by performing characterization tests around different bending angles.

7. Acknowledgment

This research is supported by Swiss National Centers for Competence in Research (NCCR) in Robotics.

References

[1] A. Firouzeh, M. Ozmaeian, A. Alasty, A. I. zad, An ipmc-made deformable-ring-like robot, Smart Materials and Structures 21 (6) (2012) 065011.

[2] A. Firouzeh, S. Yi, L. Hyunchul, J. Paik, Sensor and actuator integrated low-profile robotic origami.

[3] S. Yun Seong, S. Yi, R. van den Brand, J. von Zitzewitz, S. Micera, G. Courtine, J. Paik, Soft robot for gait rehabilitation of spinalized rodents, in: Intelligent Robots and Systems (IROS), 2013 IEEE/RSJ International Conference on, pp. 971–976.

[4] J. Paik, B. An, D. Rus, R. J. Wood, Robotic origamis: self-morphing modular robots, in: Proceedings of 2nd International Conference on Morphological Computation, 2011.

[5] A. Firouzeh, J. Paik, Facial rehabilitative device based on robogami (robotic origami) platform (09.19.2014 2014).

[6] H. Vandeparre, D. Watson, S. P. Lacour, Extremely robust and conformable capacitive pressure sensors based on flexible polyurethane foams and stretchable metallization, Applied Physics Letters 103 (20) (2013) –.

[7] R. Samuel, M. O. Benjamin, G. Todd, X. Daniel, R. S. Herbert, A. A. Iain, Self-sensing dielectric elastomer actuators in closed-loop operation, Smart Materials and Structures 22 (10) (2013) 104018.

[8] L. Viry, A. Levi, M. Totaro, A. Mondini, V. Mattoli, B. Mazzolai, L. Beccai, Flexible three-axial force sensor for soft and highly sensitive artificial touch, Advanced Materials 26 (17) (2014) 2659–2664. doi:10.1002/adma.201305064. URL http://dx.doi.org/10.1002/adma.201305064

[9] C. Gentile, M. Wallace, T. Avalon, S. Goodman, R. Fuller, T. Hall, Angular displacement sensor (11.02.1992 1992).

[10] J. K. Paik, R. K. Kramer, R. J. Wood, Stretchable circuits and sensors for robotic origami, in: Intelligent Robots and Systems (IROS), 2011 IEEE/RSJ International Conference on, pp. 414–420.

[11] D. Thuau, C. Ayela, P. Poulin, I. Dufour, Highly piezoresistive hybrid mems sensors, Sensors and Actuators A: Physical 209 (0) (2014) 161 – 168.

[12] S. Rosset, H. Shea, Flexible and stretchable electrodes for dielectric elastomer actuators, Applied Physics A 110 (2) (2013) 281–307.

[13] T. Yamada, Y. Hayamizu, Y. Yamamoto, Y. Yomogida, A. Izadi-Najafabadi, D. N. Futaba, K. Hata, A stretchable carbon nanotube strain sensor for human-motion detection, Nat Nano 6 (5) (2011) 296–301, 10.1038/nnano.2011.36.

[14] U. Tata, C. Hung, C. M. Nguyen, C. Jung-Chih, Flexible sputter-deposited carbon strain sensor, Sensors Journal, IEEE 13 (2) (2013) 444–445.

[15] N. Hu, Y. Karube, M. Arai, T. Watanabe, C. Yan, Y. Li, Y. Liu, H. Fukunaga, Investigation on sensitivity of a polymer/carbon nanotube composite strain sensor, Carbon 48 (3) (2010) 680 – 687.

[16] M. Knite, V. Teteris, A. Kiploka, J. Kaupuzs, Polyisoprene-carbon black nanocomposites as tensile strain and pressure sensor materials, Sensors and Actuators A: Physical 110 (13) (2004) 142–149.

[17] L. Wang, F. Ma, Q. Shi, H. Liu, X. Wang, Study on compressive resistance creep and recovery of flexible pressure sensitive material based on carbon black filled silicone rubber composite, Sensors and Actuators A: Physical 165 (2) (2011) 207 – 215.

[18] L. Wang, J. Li, A piezoresistive flounder element based on conductive polymer composite, Sensors and Actuators A: Physical 216 (0) (2014) 214 – 222.

[19] M. A. Lacasse, V. Duchaine, C. Gosselin, Characterization of the electrical resistance of carbon-black-filled silicone: Application to a flexible and stretchable robot skin, in: Robotics and Automation (ICRA), 2010 IEEE International Conference on, pp. 4842–4848.

[20] S. Xiaoping, D. D. L. Chung, A piezoresistive carbon filament polymer-matrix composite strain sensor, Smart Materials and Structures 5 (2) (1996) 243.

[21] Y. Wang, A. X. Wang, Y. Wang, M. K. Chyu, Q.-M. Wang, Fabrication and characterization of carbon nanotubepolyimide composite based high temperature

flexible thin film piezoresistive strain sensor, Sensors and Actuators A: Physical 199 (0) (2013) 265 – 271.

[22] A. Ferrreira, J. G. Rocha, A. Ansn-Casaos, M. T. Martnez, F. Vaz, S. Lanceros-Mendez, Electromechanical performance of poly(vinylidene fluoride)/carbon nanotube composites for strain sensor applications, Sensors and Actuators A: Physical 178 (0) (2012) 10–16.

[23] J. R. Bautista-Quijano, F. Avils, J. O. Aguilar, A. Tapia, Strain sensing capabilities of a piezoresistive mwcnt-polysulfone film, Sensors and Actuators A: Physical 159 (2) (2010) 135–140.

[24] K. Kure, T. Kanda, K. Suzumori, S. Wakimoto, Intelligent fma using flexible displacement sensor with paste injection, in: Robotics and Automation, 2006. ICRA 2006. Proceedings 2006 IEEE International Conference on, pp. 1012–1017.

[25] J. M. Engel, J. Chen, L. Chang, D. Bullen, Polyurethane rubber all-polymer artificial hair cell sensor, Microelectromechanical Systems, Journal of 15 (4) (2006) 729–736.

[26] W. Luheng, D. Tianhuai, W. Peng, Effects of conductive phase content on critical pressure of carbon black filled silicone rubber composite, Sensors and Actuators A: Physical 135 (2) (2007) 587–592.

[27] W. Luheng, L. Cheng, Piezoresistive effect of a carbon nanotube silicone-matrix composite, Carbon 71 (0) (2014) 319–331.

[28] Properties of eco-flex30 and dragon skin 30.
URL http://www.smooth-on.com/

[29] Conductive adhesives comparison table.
URL http://www.tedpella.com/adhesive_html/Adhesive-Comparison.htm